

To be submitted to Sol. Phys..

Solar Wind Forecasting with Coronal Holes

S. J. Robbins¹

Department of Astronomy, Case Western Reserve University, Cleveland, OH 44106

stuart.robbins@case.edu

and

C. J. Henney² and J. W. Harvey²

National Solar Observatory, Tucson, AZ 85719

chenney@noao.edu

ABSTRACT

An empirical model for forecasting solar wind speed related geomagnetic events is presented here. The model is based on the location and size of solar coronal holes determined with Kitt Peak Vacuum Telescope He I 1083.0 nm spectroheliograms and photospheric magnetograms. This method differs from the Wang-Sheeley model that is based on photospheric magnetograms to estimate the open field line configuration. Solar wind and coronal hole data for the period between May 1992 and September 2003 are investigated. The new model is found to be accurate to within 4.5 – 5.7% (the range depends upon the number of days ahead forecast) of observed solar wind measurements for the best one-month periods within the time frame studied. The overall correlation is as high as 0.382 for the full 11 years. Using coronal hole maps, the model can predict the solar wind velocity up to 8.5 days in advance with an average deviation as low as 9.4 – 10.0% for a given one-month period. This is further in advance forecasting and up to a factor of 2 improvement over the Wang-Sheeley model. Its main features are a strong southern hemisphere bias, sunspot cycle dependence, and

¹REU 2004 summer intern with the National Solar Observatory. The REU program is funded by the National Science Foundation.

²National Solar Observatory

that a complete forecast of up to nine days in advance can be made from a single solar image, as opposed to a full synoptic map required by the Wang-Sheeley method.

Subject headings: Sun: coronal holes, Sun: solar wind

1. Introduction

The solar wind has an important impact upon technology today, for it influences the longevity and the survival of all satellites outside and within Earth's magnetosphere as well as many ground-based electronics. In today's world, communications, power grids, and even trains are all at the mercy of space weather, governed by the ever-changing solar wind (Jansen & Pirjola 2004).

Because of the multi-billion dollar industries that rely upon these electronic devices and a quasi-static predictable nature of the atmosphere and magnetosphere, various methods have been created to shield them from dramatic increases in solar wind output and resulting effects; however, many of these rely upon a fore-knowledge of increased output, so an accurate forecast of the solar wind velocity at Earth is essential.

Presented here is an expansion of the 1970s work of Sheeley and Harvey (e.g. Sheeley & Harvey (1981)) to (1) show that coronal holes can be used to as accurately forecast solar wind velocities as synoptic maps and magnetic field propagation, (2) demonstrate the latitude and longitude weighting that leads to the best forecast for the entire 11-year period studied, (3) illustrate the dependence upon the phase of the sunspot cycle, (4) show coronal holes can also be used to forecast the interplanetary magnetic field polarity at Earth, and (5) provide example 1-month-period forecasts using this model.

1.1. Coronal Holes

Krieger, Timothy, & Roelof (1972) used data from 1970 and traced solar wind streams observed at Earth back to the Sun; they found a good agreement between high-speed solar wind velocities and the positions of coronal holes (see Figure 7, Krieger, Timothy, & Roelof (1972)). Extensive work by Sheeley and Harvey (e.g. Sheeley & Harvey (1981)) throughout the 1970s further solidified the link between coronal holes, solar wind speeds, and geomagnetic disturbances.

Coronal holes are characterized by the following: Compared with the surrounding

corona, the holes are lower in density and temperature¹, and their magnetic fields are open, weak, and divergent (Altschuler, Trotter, & Orrall 1972; Harvey & Recely 2002). They are the main sources of intense solar wind that most seriously impact geomagnetic events (Harvey & Recely 2002).

Coronal holes are mainly observed in x-ray, extreme ultra-violet, and radio wavelengths, but they can also be seen in the two chromospheric spectral lines He I D₃ and 1083 nm, and also on the limb using Fe XIV 530.3 nm and K-coronagraphs (Harvey & Recely 2002). Work here was done with images based upon the 1083 nm line.

Holes form when the remnants of active magnetic field regions, emerging in both north and south hemispheres over several months, combine and form a relatively large region of a unipolar field. Remnants of the opposite polarity fields surround the holes, forming their divergent magnetic nature (Timothy, Krieger, & Vaiana 1975).

There are three major classifications for coronal holes: Polar, non-polar, and transient. In general, polar coronal holes exist for many years, forming from non-polar holes that drift pole-ward and merge, generally soon after a solar maximum. They reach their largest area around the time of solar minimum, where they can occupy as much as 15% of the disk, and they wane and disappear around the time of the next maximum (Harvey & Recely 2002). Polar coronal hole boundaries distort over their lifetimes, and this is due to sunspot activity (Maravilla et al. 2001).

Non-polar holes are more isolated, and they are limited to a latitude range of $\pm 60^\circ$. They are associated with an active or formerly active magnetic region and generally persist for a few months - over one to several rotations (Harvey & Recely 2002). Transient holes have briefer lifetimes, generally lasting for only one to two days; they are associated with eruptive events such as flares and coronal mass ejections (Harvey & Recely 2002).

1.2. Wang-Sheeley Model

WS

Wang & Sheeley (1990) discovered an empirical relation between solar wind velocity and coronal flux-tube expansion. They found that both slow and fast solar winds have their origins in coronal holes and that their velocities are related to the open field line divergence rate close to the Sun. Their results suggested that synoptic maps can be modeled to run forward in time under the influence of differential rotation, supergranular diffusion, and meridional flow; the resulting simulated photospheric field can then be used to forecast the

¹Munro & Withbroe (1972) found the coronal temperature is lowered by $\sim 600,000$ K.

wind's velocity at Earth.

The Wang-Sheeley model was modified in 2000 by Arge & Pizzo (2000) with five main modifications; these included the establishment of a continuous empirical function that relates the magnetic expansion factor to solar wind velocity at the source surface, propagation of the solar wind from the source surface to Earth using assumptions about radial streams and their interactions, and optimization of the technique for the construction of daily updated synoptic maps from magnetogram data.

Arge & Pizzo (2000) studied a three-year period centered around the May 1996 solar minimum. Their three-year sample period had an overall correlation of ~ 0.4 with observed solar wind velocities and an average fractional deviation (see §5) of 0.15. When excluding a 6-month period with large data gaps, they correctly forecast the solar wind to within 10 – 15%. Interplanetary magnetic field (IMF) polarity was correctly forecast $\sim 75\%$ of the time.

2. Model Input Data

Solar wind velocity data was obtained from the National Space Science Data Center's OMNIWeb website. Daily averages were used because that was the approximate sampling rate of the coronal hole maps.

Coronal hole data from May 28, 1992 through September 25, 2003 (JD 2448771 – 2452908) were used; this corresponds to the last half of Cycle 22 and the first half of Cycle 23. Hand-drawn maps based upon the KPVT 1083 mm He I images and photosphere magnetograms were used (see Harvey & Recely (2002) for details on coronal hole map construction). The images were mapped into sine-latitude to create square images of equal area.

The images were keyed in such a way that the background solar disk was set to a value of 0, and each coronal hole was labeled with an integer. Each hole was signed to correspond to the polarity of the hole. In this manner, the third hole drawn on a map would be given a value of 3. If it had a negative polarity it would be changed to -3 . The total magnetic flux of each hole was written into the header of the file.

3. Solar Wind Correlation Analysis

The solar wind velocity data was taken as-is from the OMNIWeb data set. For the time period studied, it had 91.8% coverage. Missing data was filled using a cubic spline interpolation.

Each coronal hole image was read into a data array. 14°-wide latitude regions from 90° N to 90° S were taken, masking out all the surrounding pixels; this corresponded to approximately a 24-hour rotation on the Sun as seen from Earth. A 1-day-wide window was selected because anything much wider resulted in mixed temporal signals and looser correlations. The absolute value of the signed mean of each swath was taken to yield a percent coverage of the area by coronal holes. This gave a single number tied to the date the coronal hole images were taken.

The holes were not scaled by their respective magnetic flux. This was initially investigated, but it was found that the final correlation was substantially increased when the flux was not included and area was the only factor. Wang & Sheeley (1990) discovered the same effect.

This data set was then interpolated into the time frame of the solar wind velocity data in order to eliminate uncertainties generated by the temporal non-uniformity in which the coronal hole data were sampled. Because there was 68.6% coverage of the days in the 11-year time frame by the coronal holes, dates in the final time series that did not have a coronal hole map within 0.5 days were masked for all of the analysis except when cross-correlations were calculated.

Cross-correlation analyses (see Appendix A) between the two data sets were then performed to determine if and how they were related.

3.1. Data Set Scaling

Because the coronal hole data set was the percent of the solar disk covered by coronal holes, it needed to be scaled in order to give a physical value for solar wind velocity. Scaling does not affect the cross-correlation, so this allowed for the development of an appropriate scaling mechanism after proper weighting had been determined (§3.2 and 3.3).

A scatter plot of the coronal hole versus the velocity data was constructed, and a linear regression was then calculated. The coronal hole data set was multiplied by the slope of the regression, and the vertical offset was then added into the set. The resulting time series was mathematically the best fit, but the mathematical best scaling was non-physical in that it

did not result in the range of velocities observed.

Therefore, scaling was chosen by a process of minimizing the average fractional deviation and standard deviation while maintaining an accurate range for forecast values, assuming a linear relationship between the two data sets. The scaling that yielded the best agreement between the two sets was nearly identical between the three forecasting windows found in §3.2, so the average was taken. This scaling was then used in §3.4 and 5. With this scaling and the best weighting (found in the following sections), the resulting average fractional deviation for the entire 11-year data set is 1.2% with a $1-\sigma$ uncertainty of $\pm 29.5\%$.

3.2. Longitude Analysis and Forecasting Windows

23 longitude swaths were examined, starting with the first centered at 77° E and going through to the last centered on 77° W. Each of these were processed in the manner described above.

The first result is the quantification of how long solar features on the disk take to impact Earth, based upon longitude:

$$d = (3.737 \pm 0.022) - (0.07390 \pm 0.0005) \theta \quad (1)$$

where d is the delay in days and θ is the center of the longitude swath in degrees as measured from the central meridian (East is negative, West is positive); uncertainties are $1-\sigma$. The data are fit to this line in Figure 1.

Figure 2 shows the maximum cross-correlation coefficient that corresponds to the best time lag each longitude swath. Statistical significance is shown in table 1. This shows three relatively good prediction windows that were later used to forecast. They are centered on 63° E, 14° E, and 7° W. These yield forecasts of 8.5 days, 5 days, and 3.5 days, respectively.

3.3. Latitude Weighting Analysis

To improve the cross-correlation, the Sun was further divided into latitude bins; 60° increments were used, generating Northern (90° N - 30° N), Equatorial (30° N - 30° S), and Southern (30° N - 90° S) regions. A combination of Northern with Equatorial and Southern with Equatorial were used in order to have a total of five bins. The cross-correlation of each latitude bin were calculated for each of the three windows found in §3.2.

Figure 3 shows there is a very strong bias towards the southern hemisphere. For the entire 11-year time series, the correlation for the combination of the Southern with Equatorial region is almost a factor of 2 greater than that for the Northern with Equatorial region.

This southern bias was explored further by tiling 40° swaths with an overlap of 20° across the disk for a total of 8 regions; three extra were calculated in order to verify the peak's position, and the results are illustrated in Figure 4. It shows that the southern bias is centered between 10° S to 50° S, and that the benefit of going farther South decays rapidly. Going North, the fall-off in correlation is much more gradual, and it crosses into an anti-correlation around 40° N.

Based upon this, the final latitude window used for the model spans 30° N to 70° S. This resulted in a maximum cross-correlation coefficient of 0.382 for the 8.5-day forecast, 0.347 for the 5-day forecast, and 0.377 for the 3.5-day forecast throughout the entire 11-year period.

3.4. Magnetic Activity Cycle Dependence

Sheeley and Harvey's work from the 1970s (e.g. Sheeley & Harvey (1981)) hinted at a dependence upon the sunspot cycle for the correlation between the coronal holes and solar wind. This was quantitatively explored for the time period the coronal hole data set spans - the last half of Cycle 22 and the first half of Cycle 23. The full time series was divided into six time subsets of approximately 690 days each, shown in table 2 and illustrated in Figure 5 with sunspot counts overlaid.

Figure 6 shows the results of this analysis. There is a strong dependence upon the phase of the sunspot cycle, similar to the qualitative results of Sheeley and Harvey. The correlation is best during and just after solar maximum, and it is worst during solar minimum and the beginning ascending phase of the Cycle.

4. Interplanetary Magnetic Field Polarity Forecast

In addition to forecasting the solar wind velocity, coronal hole maps can be used to predict the interplanetary magnetic field (IMF) polarity at Earth. The 3.5-day forecast window at 7° W was used for this.

The coronal hole maps were scaled so that each pixel with a positive polarity hole had a value of +1 and each pixel with a negative polarity hole had a value of -1; the background

solar disk was set to 0. The mean of all the pixels in the 14°-wide region was taken with a latitude range of $\pm 60^\circ$.

Excluding days when the average was very close to 0 and the two data sets both did not have actual measurements, 47.3% of the days in the 11-year time series were forecast; of those, 73.6% of them had the IMF polarity correctly forecast. When only excluding days that did not have both velocity and coronal hole data, the IMF polarity was forecast 62.9% of the days, and of this it was correctly forecast 68.7% of the days that could be forecast. This is a drop of 5% in accuracy, but an increase by 15% of the days forecast.

This is slightly lower than the results Arge & Pizzo (2000); they correctly forecast the polarity 75% of all the days in their three-year time period.

5. Example Forecasts

There are several ways to compare this empirical model with the modified Wang-Sheeley (Arge & Pizzo 2000). The first is by looking at cross-correlations.

Arge & Pizzo (2000) studied a three-year period. For this period, they found - using their best forecast method - a correlation of 0.389. For the same time length of three years, the model presented here has a maximum cross-correlation of 0.439 – 0.473 with the range depending upon the length of the forecast made. The entire 11 years had a correlation of 0.347 – 0.382.

The best one-month period presented by Arge & Pizzo (2000) had a cross-correlation coefficient of 0.813. The best one-month period within the 11-year series that was studied for this paper had a correlation of 0.864 – 0.894 with the range again dependent upon which of the three forecasts was used.

A second way to judge the effectiveness of this as a forecast tool is through comparing the average fractional deviation (AFD), defined as $\langle \frac{\text{prediction} - \text{observed}}{\text{observed}} \rangle$, where a value of 0 indicates a perfect match. Arge & Pizzo (2000) had an AFD that averaged at 0.159 with a range of about 0.15 for the entire three-year period. The best AFD for the best one-month period presented in their paper is 0.096. For the entire 11-year period studied in this paper, the AFD had a mean of 0.00059 – 0.00740 with a standard deviation of 0.293 – 0.306. The best AFD of a one-month period studied here is 0.00055 – 0.00126.

Finally comes the practical test of forecasting the solar wind. Figures 7 and 8 present two sample forecast periods spanning approximate one-month time frames. Fig. 7 shows one of the best periods while Figure 8 represents one of the worst periods for this model.

Note

Besides the purpose of demonstrating the practicality of this method through sample forecasts, an important statistical point was discovered. Arge & Pizzo (2000) argue that the correlation coefficients are sometimes poor indicators of how well the model predicts the solar wind velocity. However, when searching for sample periods to include in this paper by looking at the lowest AFD - as they argue is the better indicator - it was found that the AFDs closest to 0 were for time periods where the solar wind velocity was near a minimum, but still varied, and the forecast was a flat line (such as illustrated around JD 2450350 in Figure 8). In order to find periods where the forecast mirrored the observed values, the cross-correlations were used.

This is illustrated within the two forecasts themselves. The correlations for the good period are between 0.748 – 0.807 while those for the poor period are 0.069 – 0.207. Statistical significance levels are given in table 1. The AFD for the good period is in the range –0.167 – –0.124 while that for the poor period lies between –0.116 – –0.0935. When $\pm\sigma$ uncertainties are applied (see §3.1; uncertainties are not shown in the Figures due to size and readability constraints), the good period is correctly predicted for every day forecast, while the poor period has over one dozen forecasts that do not cover the observed values. It is thus concluded that, in general, correlation coefficients are more telling of the forecast's accuracy than AFD.

6. Discussion

For the 11 years studied, this empirical model is a quantitative improvement over one of the most widely used forecasting methods of solar wind velocity - the Wang-Sheeley. Both are based in the empirical relation between coronal holes and the solar wind, but the Wang-Sheeley treatment is to propagate the magnetic fields to create the forecast. The method presented here is with simple weighting of the solar disk in order to create a forecast for the solar wind velocity at Earth.

There are several important and unique characteristics of this empirical model. First, it relies upon a strong southern weighting that has yet to be explained. Weighting the south while removing the northern regions of the Sun results in correlations over a factor of 2 higher than a flat weight. The final weighting shows higher cross-correlations than those found in the leading modified version of the Wang-Sheeley model, presented in Arge & Pizzo (2000). Second, there is a strong dependence upon the phase of the sunspot cycle. This has been found in the past, and we hope to explore it further when more data becomes available in the future. It can also be used to predict the magnetic field polarity at Earth from the sun.

Another important feature of this model is its lack of dependence upon synoptic maps,

and that a forecast can be created from a single image of the solar disk. There are three prime forecast windows centered at 63° E, 14° E, and 7° W that offer forecasts of 8.5, 5, and 3.5 days respectively, but any 14°-wide window (approximately one day's solar rotation as seen by Earth) can be used and the forecast in days can be obtained for that area via Equation 1. With multiple prime forecast windows, this method is less sensitive to gaps in observations because of the overlap that is offered of forecast times with gaps in coronal hole sampling.

Solar wind data is available online at <http://nssdc.gsfc.nasa.gov/omniweb/>. This work is carried out through the National Solar Observatory Research Experiences for Undergraduate (REU) site program, which is co-funded by the Department of Defense in partnership with the National Science Foundation REU Program. This research was supported in part by the Office of Naval Research Grant N00014-91-J-1040. The National Solar Observatory is operated by AURA, Inc. under a cooperative agreement with the National Science Foundation.

Facilities: KPNO.

A. Cross-Correlation

Equation A1 is the basic form of the cross-correlation used in this study.

$$\rho_{xy} = \begin{cases} \frac{\sum_{k=0}^{N-|L|-1} (x_{k+|L|} - \bar{x})(y_k - \bar{y})}{\sqrt{\left(\sum_{k=0}^{N-1} (x_k - \bar{x})^2\right) \left(\sum_{k=0}^{N-1} (y_k - \bar{y})^2\right)}} & \text{for } L < 0 \\ \frac{\sum_{k=0}^{N-L-1} (x_k - \bar{x})(y_{k+L} - \bar{y})}{\sqrt{\left(\sum_{k=0}^{N-1} (x_k - \bar{x})^2\right) \left(\sum_{k=0}^{N-1} (y_k - \bar{y})^2\right)}} & \text{for } L \geq 0 \end{cases} \quad (\text{A1})$$

In Equation A2, $P_N(|r| \geq |r_0|)$ gives the probability that with N observations, two uncorrelated random sets of variables would give a coefficient r as large as r_0 . Therefore, a correlation was considered to be significant if the coefficient obtained fell in $P_N \leq 5\%$. If it was less than 1%, then the correlation was highly significant.

$$P_N(|r| \geq |r_0|) = \frac{2\Gamma((N-1)/2)}{\sqrt{\pi}\Gamma((N-2)/2)} \int_{|r_0|}^1 (1-r^2)^{(N-4)/2} dr \quad (\text{A2})$$

For comparisons with other studies and to demonstrate features of this model, the significance of several values for N were calculated, and they are listed in table 1.

REFERENCES

- Altschuler, M. D., Trotter, D. E., and F. Q. Orrall: 1972, *Sol. Phys.*, 26, 354.
- Arge, C. N. and V. J. Pizzo: 2000, *J. Geophys. Res.*, 105:A5, 10,465.
- Harvey, K. L. and F. Recely: 2002, *Sol. Phys.*, 211, 31.
- Jansen, F. and R. Pirjola: 2004, *Eos*, 85:25, 241.
- Krieger, A. S., Timothy, A. F., and E. C. Roelof: 1972 *Sol. Phys.*, 29, 505.
- Maravilla, D. et al.: 2001, *Sol. Phys.*, 203, 27.
- Munro, R. H. and G. L. Withbroe: 1973, *ApJ*, 176, 511.
- Sheeley, N. R., Jr. and J. W. Harvey: 1980, *Sol. Phys.* 70, 237.
- Timothy, A. F., Krieger, A. S., and G. S. Vaiana: 1975, *Sol. Phys.*, 42, 135.
- Yang, Y.-M. and N. R. Sheeley, Jr.: 1990, *ApJ*, 355, 726.

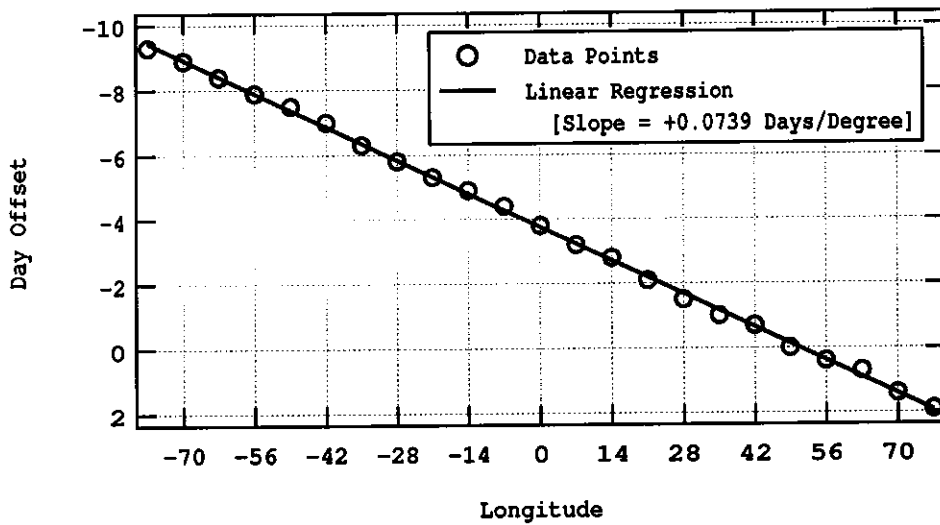


Fig. 1. Day Offset with Solar Disk Latitude: A linear relation was found in the lag before affects of the coronal holes within 14°-wide swaths of the solar disk are observed at Earth upon the solar wind velocity. Shown here are the data for this plotted along with the best linear fit. Negative longitude corresponds to East and positive to West with 0 being the central meridian.

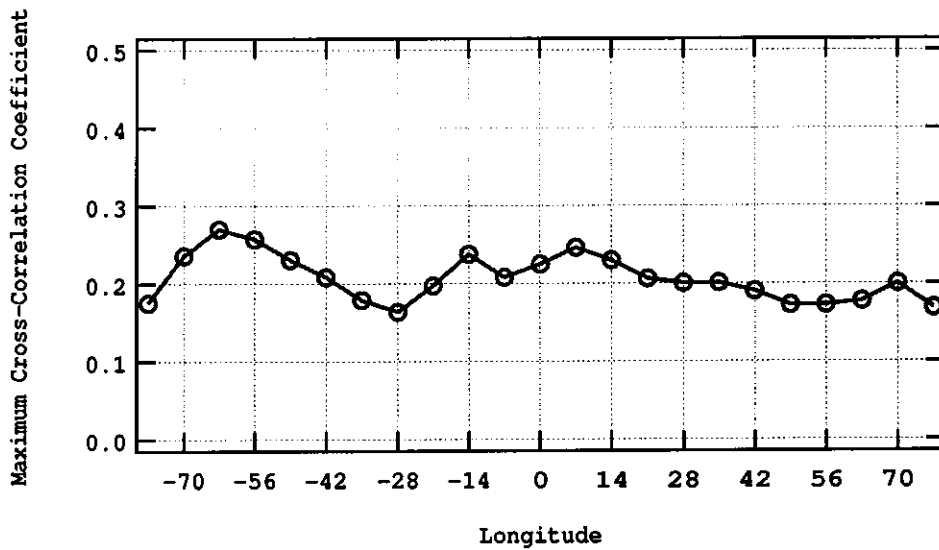


Fig. 2.— Longitude Cross-Correlations: 14°-wide swaths of the solar disk were tiled across the solar surface with 7° overlap between successive swaths. The maximum cross-correlation (corresponding to a day offset described by Equation 1 and shown in Figure 1) of the resulting data set with the solar wind velocity data are shown here. Negative longitude corresponds to East and positive to West. This shows three relatively good forecast windows centered on 63° E, 14° E, and 7° W.

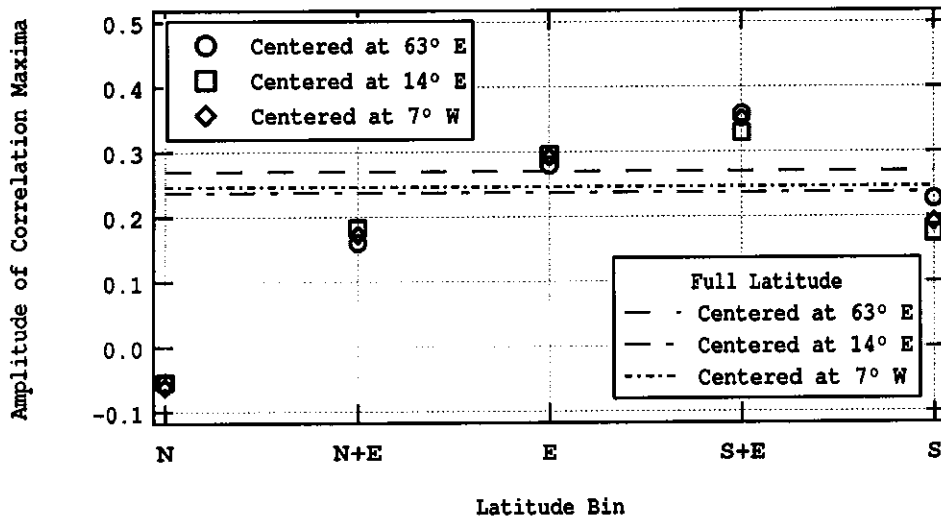


Fig. 3.— **Five Latitude Regions:** The three longitude forecasts' cross-correlations with the solar disk divided into five latitude regions described in §3.3 is shown. This clearly indicates there is a strong preference for the southern region of the Sun for an accurate forecast of the solar wind. This is refined in Figure 4.

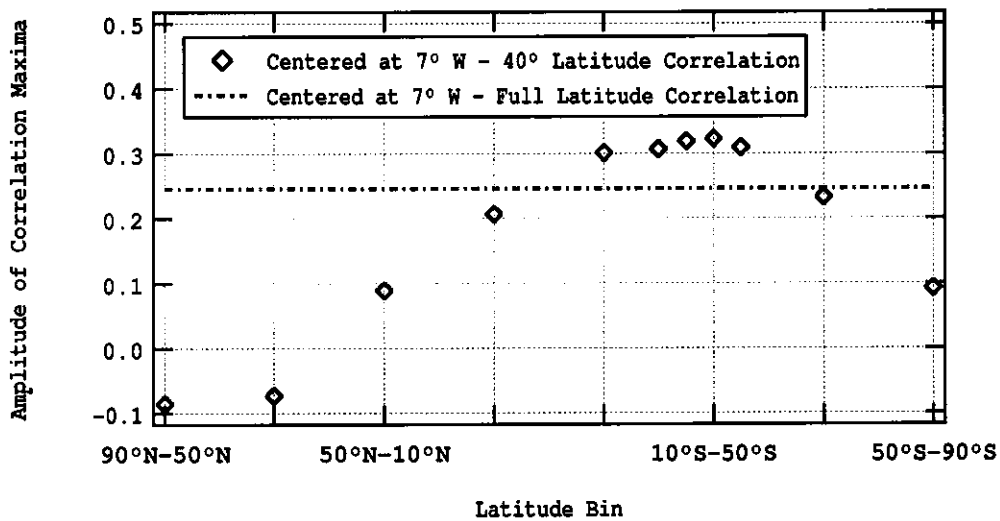


Fig. 4.— **40° Latitude Swath Correlations:** Refined is the 7° W forecast window for 11 different latitude regions, each 40° wide (described in §3.3). From this, the southern bias that was discovered with Figure 3 is refined to show that it is centered around 30° S. The rapid fall-off south of this led to the refinement of the final latitude window to 30° N through 70° S. This region was chosen in order to avoid too much tailoring to a specific time period.

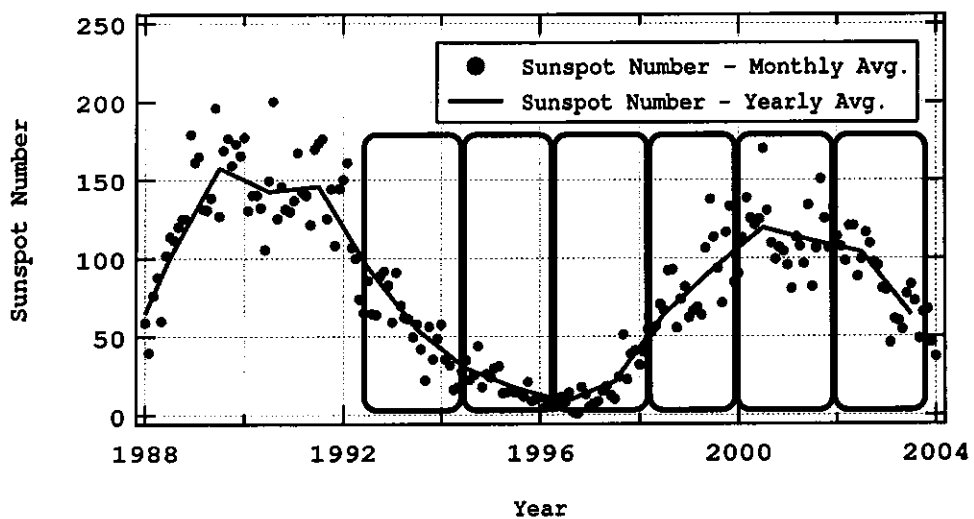


Fig. 5.— Sunspot Cycle: Both monthly and yearly sunspot number averages are shown here along with six time bins into which the 11-year data set was divided; the six bins are indicated by the rounded rectangles, are numbered 1 – 6 left to right, and lasted approximately 690 days each (see table 2).

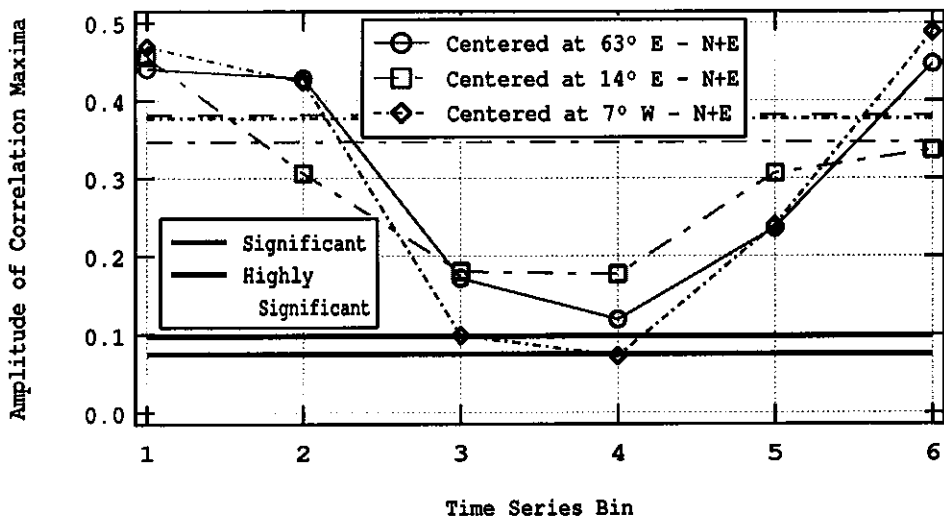


Fig. 6.— Cycle Correlations: Divided into the six time bins (see Figure 5 and table 2), the cross-correlations of the coronal hole data with the solar wind follows the sunspot cycle well, with the correlation being very high during solar maximum and the beginning decline from maximum, and the correlation reaching a minimum during solar minimum. Each of the three forecast windows are shown here; the window centered on 7° W shows the largest variation in correlation, going from nearly 0.5 to statistical insignificance (see Equation A2 and table 1), while the window centered at 14° E shows the least variation with the Cycle.

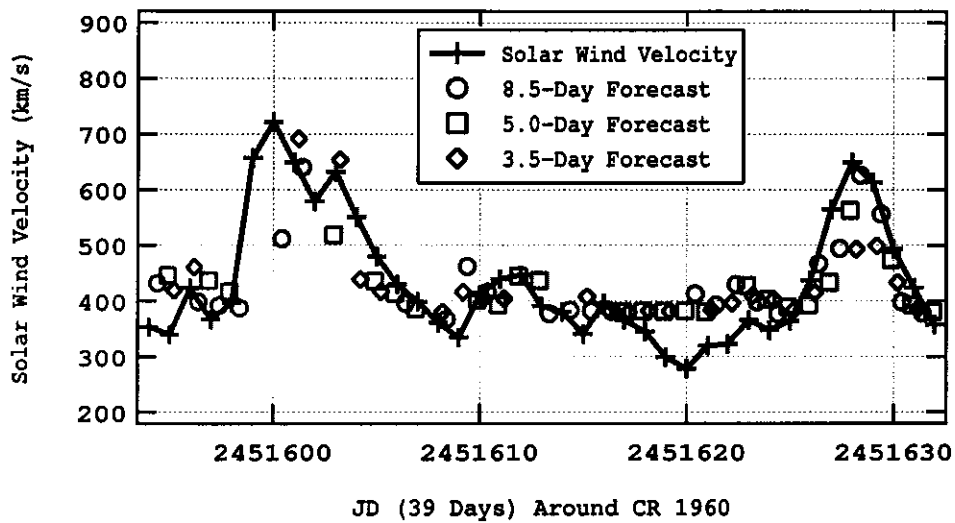


Fig. 7.— **Good Forecast Period:** JD 2451594 – 2451632 has a cross-correlation coefficient of 0.748, 0.807, and 0.793 for the 8.5-, 5-, and 3.5-day forecasts respectively. For this number of days, the correlation is considered significant if above 0.32 and highly significant if above 0.41. The AFD during this period is -0.167 ± 0.158 , -0.124 ± 0.186 , and -0.124 ± 0.161 . This period is from time bin 5 (see Figure 5).

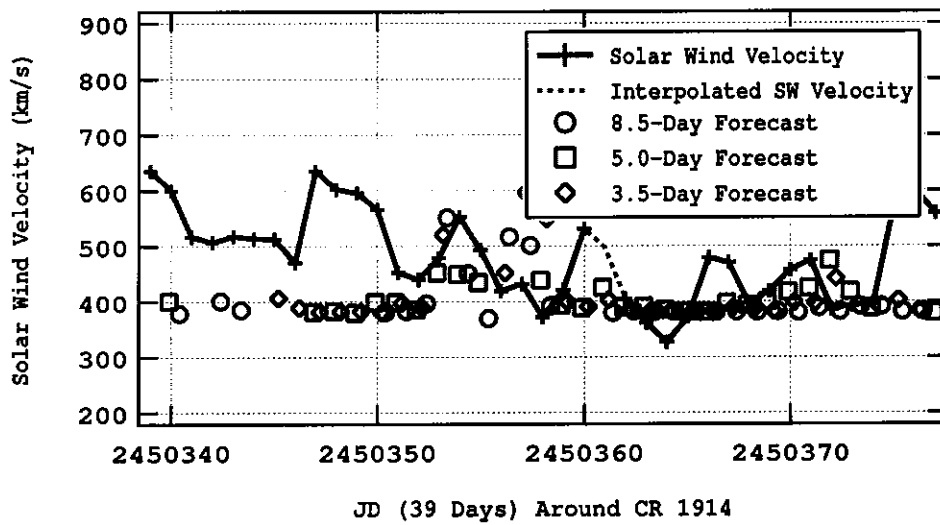


Fig. 8. **Poor Forecast Period:** JD 2450339 – 3450377 has a cross-correlation coefficient of 0.207, 0.121, and 0.0685 for the 8.5-, 5-, and 3.5-day forecasts respectively. For this number of days, the correlation is considered significant if above 0.32 and highly significant if above 0.41. The AFD during this period is -0.0935 ± 0.1771 , -0.1161 ± 1619 , and -0.0976 ± 0.2055 . This period is from time bin 3 (see Figure 5).

Table 1: Significance for various time series lengths, as determined with Equation A2.

Number of Days	Significant if Above	Highly Significant if Above
30	0.36	0.46
39	0.32	0.41
365	0.10	0.14
688	0.074	0.098
690	0.074	0.098
4138	0.031	0.040

Table 2: Time series subdivisions of full JD 2448771 – 2452908 used in cross-correlations.

Julian Date Range	Date	Days	Days with Data	Completeness
2448771 – 2449460	May 28, 1992 - Apr 17, 1994	690	456	66.1%
2449461 – 2450150	Apr 18, 1994 - Mar 7, 1996	690	472	68.4%
2450151 – 2450840	Mar 8, 1996 - Jan 26, 1998	690	498	72.2%
2450841 – 2451530	Jan 27, 1998 - Dec 17, 1999	690	509	73.8%
2451531 – 2452220	Dec 18, 1999 - Nov 6, 2001	690	446	64.6%
2452221 – 2452908	Nov 7, 2001 - Sep 25, 2003	688	456	66.3%
2448771 – 2452908	May 27, 1992 - Sep 25, 2003	4138	2838	68.6%